Atom-Light Hybrid Quantum Gyroscope

Yuan Wu,[1] Jinxian Guo,[2,3] Xiaotian Feng,[1] L.Q. Chen◉,[1,3,*] Chun-Hua Yuan◉,[1,†] and
Weiping Zhang[2,3,4]

[1] *State Key Laboratory of Precision Spectroscopy, Quantum Institute of Atom and Light, Department of Physics,*
East China Normal University, Shanghai 200062, People's Republic of China

[2] *School of Physics and Astronomy, and Tsung-Dao Lee Institute, Shanghai Jiao Tong University,*
Shanghai 200240, People's Republic of China

[3] *Shanghai Research Center for Quantum Sciences, Shanghai 201315, People's Republic of China*

[4] *Collaborative Innovation Center of Extreme Optics, Shanxi University, Taiyuan, Shanxi 030006,*
People's Republic of China

An atom-light hybrid quantum gyroscope (ALHQG) is proposed due to its high rotation sensitivity. It consists of an optical Sagnac loop to couple rotation rate and an atomic ensemble as quantum beam splitter (recombiner) [QBS(C)] based on atomic Raman-amplification process to realize the splitting and recombination of the optical wave and the atomic spin wave. The rotation sensitivity can be enhanced by the quantum correlation between Sagnac loop and QBS(C). The optimal working condition is investigated to achieve the best sensitivity. The numerical results show that the rotation sensitivity can beat the standard quantum limit (SQL) in ideal condition. Even in the presence of the attenuation under practical condition, the best sensitivity of the ALHQG can still beat the SQL and is better than that of a classical fiber optic gyroscope. Such an ALHQG could be practically applied for modern inertial navigation system.

I. INTRODUCTION

Highly accurate and precise rotation-measuring instruments are fundamental apparatus in inertial navigation, geophysical studies, and tests of general relativity [1]. Rotation sensors based on the Sagnac effect [2] have been constructed using light wave and matter wave (neutrons, neutral atoms, and electrons). The Sagnac phase [3,4] is caused by an interferometer rotating at rate Ω, which is related with the velocity of the particle v, the loop area A, and the wavelength λ. Regarding the matter-wave gyroscope, such as the atomic gyroscope [5], it has large rotation sensitivity per unit area [6,7] and realizes high rotation sensitivity [8]. However, it possesses a small bandwidth and suffers from low repetition rate and dead times during which no inertial measurement can be made [9]. The light-wave gyroscope, such as a fiber optic gyroscope (FOG) [10], has large loop area, simple system, and also realizes high sensitivity, but its rotation sensitivity is limited by the SQL [11] when no quantum metrology techniques are applied (see Appendix). The limitations of the matter-wave and light-wave gyroscopes affect their practical application and further performance improvement.

To improve the performance of the matter-wave and light-wave gyroscopes, some hybrid strategies have been reported. One strategy is based on the combination of the mechanical sensor and the atomic sensor [12,13] to overcome the limitations of low bandwidth and the dead-time issue in an atomic sensor. Another strategy, such as the electromagnetically induced transparency (EIT) in a cold atomic system, has been proposed to realize the associated momentum transfer from light to atom to enhance the sensitivity of a light-wave sensor [14]. However, the sensitivity of the above hybrid strategies was limited by the SQL [15]. Because there was no quantum correlation in Sagnac loop or hybrid sensors.

Recently, some quantum metrology techniques have been proposed to enhance the sensitivity and break through SQL. One possible way is the use of quantum resources. The FOG with squeezed vacuum [16,17] and entangled NOON state [18] injection were separately demonstrated to enhance the sensitivity to beat SQL. Another possible way is the use of nonlinear processes, such as four-wave mixing (FWM) or an optical parametric amplifier, instead of the linear beam splitters, to generate correlated pairs. In 2017, a Sagnac rotation sensor based on FWM was proposed [19]. Such a sensor can beat the SQL in an ideal case due to quantum correlation between two Sagnac beams, while its practical situation has been poorly discussed. Furthermore, it is difficult to realize

―――――――
*lqchen@phy.ecnu.edu.cn
†chyuan@phy.ecnu.edu.cn

the Sagnac loop and phase stabilization for four beams [20]. Currently, a hybrid atom-light interferometer [21] has been demonstrated where Raman-amplification processes in atomic ensemble act as QBS(C) of optical wave and atomic system. The quantum correlation between optical wave and atomic ensemble leads to a high-contrast interference fringe. The phase sensitivity of the interferometer can beat the SQL by the factor of the amplification gain of the QBS(C) in principle [22].

In this work, an atom-light hybrid quantum gyroscope (ALHQG) is proposed. It is an optical Sagnac interferometer with the beam splitter (recombiner) replaced by QBS(C) to realize the quantum correlation between the Sagnac loop and QBS(C). The rotation sensitivity is analyzed with practical parameters in real experiment, including the particle number of the input field, the gain of the Raman-amplification process, the Sagnac-fiber-loop length, the attenuation coefficient of photon and atom, etc. It is found that, due to quantum correlation, the rotation sensitivity of the proposed gyroscope can beat the SQL in an ideal case. Even if the optical loss and atomic decoherence are considered in the ALHQG, the sensitivity can still beat the SQL and is better than the classical FOG with the same rotation-sensitive particle number. Such an ALHQG has a significantly practical value in quantum metrology.

The paper is organized as follows: in Sec. II, the working principle of the ALHQG in practice is described. In Sec. III, the sensitivity of the ALHQG is analyzed to have optimal working condition. In Sec. IV, the intensity and the frequency fluctuation of the laser are analyzed under optimal working condition. In Sec. V, a summary of our results is concluded.

II. THEORY AND PRINCIPLES OF ALHQG

The scheme of the ALHQG is shown in Fig. 1(a). It consists of an optical Sagnac loop to couple rotation rate Ω and an atomic ensemble as QBS(C) to generate the quantum correlated optical and atomic waves and then recombine the waves for interference. The energy levels of atom are given in Fig. 1(b). A strong Raman write beam $A_{p,1}$ and a weak Stokes input field $\hat{a}_0$ with orthogonal polarizations interact with a Λ-shaped atomic ensemble to generate an amplified Stokes field $\hat{a}_1$ and a correlated atomic spin wave $\hat{S}_1$ via the first Raman amplification. The optical field $\hat{a}_1$ and atomic spin wave $\hat{S}_1$ have quantum correlation and the relative intensity fluctuations are squeezed [19]. After interaction, the atomic spin wave $\hat{S}_1$ stays in the atomic ensemble while the Stokes field $\hat{a}_1$ and the strong Raman write beam $A_{p,1}$ travel together out of the atomic ensemble and propagate in the opposite directions inside a fiber Sagnac loop. As a result, the lights in clockwise (CW) and counterclockwise (CCW) experience a Sagnac phase induced by the rotation rate Ω. Then the Stokes field $\hat{a}_2$ and the strong Raman write beam $A_{p,2}$ recombine with
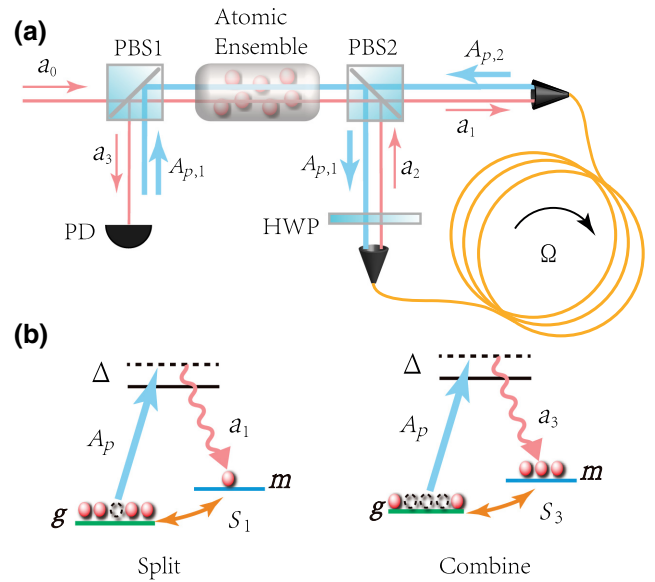

FIG. 1. (a) Schematic of the ALHQG. Red, Stokes field; blue, Raman write field; PBS, polarization beam splitter; HWP, half-wave plate to rotate the polarization angles by 90°; FC, fiber coupler; SMF, single-mode fiber; PD, photodetectors. (b) Energy levels of the atom. The lower two energy states $|g\rangle$ and $|m\rangle$ are the hyperfine split ground states. The higher-energy states $|e\rangle$ are the excited states. Δ is the single photon detuning. A strong Raman write beam $A_{p,1}$ ($A_{p,2}$) couples the state $|e\rangle$ with $|g\rangle$ and generates a Stokes field $\hat{a}_1$ ($\hat{a}_3$) and the corresponding atomic spin wave $\hat{S}_1$ ($\hat{S}_3$). The atomic spin wave stays in the cell, and the Stokes field travels out together with the pump field.

the waiting atomic spin wave $\hat{S}_2$, evolved from $\hat{S}_1$, in the atomic ensemble to realize the interference between optical wave $\hat{a}_2$ and atomic wave $\hat{S}_2$ via the second Raman amplification. Finally, the Stokes field $\hat{a}_3$ and correlated atomic spin wave $\hat{S}_3$ are generated. Therefore, the realization of ALHQG needs three steps, which are atom-light beam splitting via the first Raman process, Sagnac effect, and atom-light beam combination via the second Raman process to achieve the rotation rate Ω.

In general, the input-output relation for the atom-light beam splitting via Raman process is written as [22]

$$\widehat{a}_1 = G_1\widehat{a}_0 + e^{i\theta_1}g_1\hat{S}_0^\dagger, \tag{1}$$

$$\widehat{S}_1 = e^{i\theta_1}g_1\hat{a}_0^\dagger + G_1\widehat{S}_0. \tag{2}$$

Here $e^{i\theta_1} = \eta A_{p,1}/|\eta A_{p,1}|$, where η is the coupling constant. $G_1 = \cosh(|\eta A_{p,1}|t)$ and $g_1 = \sinh(|\eta A_{p,1}|t)$ are the amplitude gains of the first Raman-amplification process, satisfying $|G_1|^2 - |g_1|^2 = 1$. Here t is the pulse duration of pump field. $\widehat{a}_0$ and $A_{p,1}$ are initial input Stokes beam and the Raman write beam. When a coherent state $\hat{a}_0$ enters into the gyroscope and the spin wave $\widehat{S}_0$ is initially in a

vacuum state, the particle number of the input Stokes field in a single shot is $\langle \hat{a}_0^\dagger \hat{a}_0 \rangle \equiv N_{in}$. And thus, the total particle number N_{tot} inside the ALHQG include not only the photon number but also the atomic collective excitation number, which is

$$N_{tot} = \langle \hat{a}_1^\dagger \hat{a}_1 \rangle + \langle \hat{S}_1^\dagger \hat{S}_1 \rangle$$
$$= g_1^2(1 + N_{in}) + g_1^2 + G_1^2 N_{in}. \quad (3)$$

Here $\langle \rangle$ is a quantum expectation value. When $N_{in} \gg 1$, $N_{tot} \approx (g_1^2 + G_1^2)N_{in}$.

After the beam-splitting process, the optical wave $\hat{a}_1$ and the Raman write beam $A_{p,1}$ transfer out of the atomic ensemble and enter the Sagnac loop to be subject to the phase (φ_{CW} and φ_{CCW}) induced by the rotation Ω. Here φ_{CW} and φ_{CCW} are the phases of the CW and CCW induced by rotation rate, respectively. Under the influence of the optical fiber loss and the atomic decoherence, the input-output relation in the Sagnac loop is

$$\hat{a}_2 = \sqrt{T} \hat{a}_1 e^{i\varphi_{CW}} + \sqrt{R} \hat{V}_{CW}, \quad (4)$$

$$A_{p,2} = \sqrt{T} e^{i\varphi_{CCW}} A_{p,1}, \quad (5)$$

$$\hat{S}_2 = \hat{S}_1 e^{-\Gamma\tau} + \hat{F}, \quad (6)$$

where $T = \exp(-\alpha_T L)$ and $R = 1 - T$ are the transmission and reflectance coefficients of the photons, respectively. Here α_T is the fiber attenuation coefficient and L is the length of fiber loop. $\hat{V}_{CW}$ is the operator of the vacuum. $e^{-\Gamma\tau}$ is the collisional dephasing of atomic excitation and Γ is the corresponding decay rate. $\hat{F}$ is the Langevin operator and satisfies $\langle \hat{F} \hat{F}^\dagger \rangle = 1 - e^{-2\Gamma\tau}$.

Then, $\hat{a}_2$ and $A_{p,2}$ recombine with the correlated $\hat{S}_2$ via the second Raman amplification to obtain the final outputs $\hat{a}_3$ and $\hat{S}_3$, which are

$$\hat{a}_3 = G_2 \hat{a}_2 + e^{i(\theta_2 + \varphi_{CCW})} g_2 \hat{S}_2^\dagger, \quad (7)$$

$$\hat{S}_3 = e^{i(\theta_2 + \varphi_{CCW})} g_2 \hat{a}_2^\dagger + G_2 \hat{S}_2, \quad (8)$$

where $e^{i(\theta_2 + \varphi_{CCW})} = \eta A_{p,2} / |\eta A_{p,2}|$. $G_2 = \cosh(|\eta A_{p,2}| t)$ and $g_2 = \sinh(|\eta A_{p,2}| t)$ are the amplitude gains of the second Raman-amplification process, which also satisfy $|G_2|^2 - |g_2|^2 = 1$. And thus, the final outputs are

$$\hat{a}_3 = A_1 \hat{a}_0 + B_1 \hat{S}_0^\dagger + C_1 \hat{V}_{CW} + D_1 \hat{F}^\dagger, \quad (9)$$

$$\hat{S}_3 = A_2 \hat{a}_0^\dagger + B_2 \hat{S}_0 + C_2 \hat{V}_{CW}^\dagger + D_2 \hat{F}, \quad (10)$$

where

$$A_1 = \sqrt{T} G_1 G_2 e^{i\varphi_{CW}} + g_1^* g_2 e^{-\Gamma\tau} e^{i(\varphi_{CCW} + \theta_2 - \theta_1)},$$
$$B_1 = \sqrt{T} g_1 G_2 e^{i(\varphi_{CW} + \theta_1)} + G_1^* g_2 e^{-\Gamma\tau} e^{i(\varphi_{CCW} + \theta_2)},$$
$$C_1 = \sqrt{R} G_2, \ D_1 = g_2 e^{i(\varphi_{CCW} + \theta_2)},$$
$$A_2 = \sqrt{T} G_1^* g_2 e^{i(\theta_2 + \varphi_{CCW} - \varphi_{CW})} + g_1 G_2 e^{-\Gamma\tau} e^{i\theta_1},$$
$$B_2 = \sqrt{T} g_1^* g_2 e^{i(\theta_2 - \theta_1 + \varphi_{CCW} - \varphi_{CW})} + G_1 G_2 e^{-\Gamma\tau},$$
$$C_2 = \sqrt{R} g_2 e^{i(\theta_2 + \varphi_{CCW})}, \ D_2 = G_2.$$

Normally, there are two detection methods, homodyne detection and intensity detection, to detect the output and obtain the rotation rate Ω. In experiment, the operation of intensity detection is simpler. And thus, the photon-number operator $\langle \hat{n} \rangle = \langle \hat{a}_3^\dagger \hat{a}_3 \rangle$ is employed as the measurable operator in intensity detection, which is

$$\langle \hat{n} \rangle = |A_1|^2 N_{in} + |B_1|^2, \quad (11)$$

where $|A_1|^2 = T |G_1|^2 |G_2|^2 + |g_1|^2 |g_2|^2 e^{-2\Gamma\tau} + 2\sqrt{T} |G_1| |G_2| |g_1| |g_2| e^{-\Gamma\tau} \cos(\beta\Omega + \theta_1 - \theta_2)$, $|B_1|^2 = T |g_1|^2 |G_2|^2 + |G_1|^2 |g_2|^2 e^{-2\Gamma\tau} + 2\sqrt{T} |G_1| |G_2| |g_1| |g_2| e^{-\Gamma\tau} \cos(\beta\Omega + \theta_1 - \theta_2)$. Here $\beta\Omega = \varphi_{CW} - \varphi_{CCW}$ is the Sagnac phase, where $\beta = 2\pi DL/(\lambda c)$, D is the diameter of the Sagnac loop, L is the length of the Sagnac loop, and c is the speed of light in vacuum.

Based on the error-propagation analysis [22], the rotation sensitivity $\Delta\Omega$ in a single shot is defined as

$$\Delta\Omega = \frac{\langle (\Delta\hat{n})^2 \rangle^{1/2}}{|\partial \langle \hat{n} \rangle / \partial\Omega|}, \quad (12)$$

where $\langle (\Delta\hat{n})^2 \rangle = \langle \hat{n}^2 \rangle - \langle \hat{n} \rangle^2$. The uncertainty $\langle (\Delta\hat{n})^2 \rangle$ and the slope $|\partial \langle \hat{n} \rangle / \partial\Omega|$ are, respectively, given by

$$\langle (\Delta\hat{n})^2 \rangle = |A_1|^4 N_{in} + (|A_1|^2 N_{in} + |B_1|^2) |C_1|^2$$
$$+ [|A_1|^2 (1 + N_{in}) + |C_1|^2] |D_1|^2 (1 - e^{-2\Gamma\tau})$$
$$+ |A_1|^2 |B_1|^2 (1 + N_{in}), \quad (13)$$

$$\left| \frac{\partial \langle \hat{n} \rangle}{\partial\Omega} \right| = 2\sqrt{T} \beta |G_1| |G_2| |g_1| |g_2| e^{-\Gamma\tau} |\sin(\beta\Omega)| (N_{in} + 1). \quad (14)$$

When $\theta_1 - \theta_2 = \pi$, we have $|A_1|^2 = T |G_1|^2 |G_2|^2 + |g_1|^2 |g_2|^2 e^{-2\Gamma\tau} - 2\sqrt{T} |G_1| |G_2| |g_1| |g_2| e^{-\Gamma\tau} \cos(\beta\Omega)$, $|B_1|^2 = T |g_1|^2 |G_2|^2 + |G_1|^2 |g_2|^2 e^{-2\Gamma\tau} - 2\sqrt{T} |G_1| |G_2| |g_1| |g_2| e^{-\Gamma\tau} \cos(\beta\Omega)$, $|C_1|^2 = R G_2^2$, and $|D_1|^2 = g_2^2$. It

can be seen that the sensitivity is related with input particle number (N_{in}), gains (G_1, G_2, g_1, and g_2), loop length (L), rotation rate (Ω), photon-loss coefficient (α_T) and atomic decoherence rate (Γ). To obtain the best sensitivity, the discussion in the next section is focused on the optimal working condition of ALHQG.

III. SENSITIVITY ANALYSIS

Based on the above analysis, the sensitivity is related with several parameters. To simplify the analysis, we start

by the sensitivity under the ideal condition, $G_2 = G_1 = G$, $g_2 = g_1 = g$, $\theta_1 - \theta_2 = \pi$, $T = 1$, $R = 0$, and $e^{-\Gamma\tau} = 1$. With $N_{in} \gg 1$, based on Eq. (12), the rotation sensitivity $\Delta\Omega$ in a single shot is given by

$$\Delta\Omega \approx \frac{1}{M} \frac{1}{\beta\sqrt{N_{in}}}, \tag{15}$$

with

$$M = \frac{2 |Gg|^2 |\sin(\beta\Omega)|}{\sqrt{\{1 + 2|Gg|^2 [1 - \cos(\beta\Omega)]\}\{1 + 4|Gg|^2 [1 - \cos(\beta\Omega)]\}}}.$$

It can be seen that the rotation sensitivity $\Delta\Omega$ of ALHQG is inversely proportional to M and $\sqrt{N_{in}}$. $1/(\beta\sqrt{N_{in}})$ is the SQL of the classical gyroscope when the input particle number is N_{in}. Hence, based on Eq. (15), we can see that, with the same input particle number N_{in}, the ALHQG is enhanced by $1/M$ [$M > 1$ when $G > 1$ and $\cos(\beta\Omega) \to 1$] compared with the classical gyroscope. This is due to the quantum correlation between $\hat{a}_1$ and $\hat{S}_1$ in first Raman process, so that the signal-to-noise ratio is enhanced in the second Raman amplification [22].

Normally, to ensure a fair comparison, the particle number in SQL should be the rotation-sensitive particle number, which is N_{tot} in the ALHQG. Then the corresponding SQL is $\Delta\Omega_{SQL} = 1/(\beta\sqrt{N_{tot}})$ and the sensitivity enhancement factor K is

$$K = \frac{\Delta\Omega}{\Delta\Omega_{SQL}} \simeq \frac{\sqrt{g^2 + G^2}}{M}. \tag{16}$$

It can be seen that K depends only on G and $\beta\Omega$ but not N_{in}. When $K < 1$, the sensitivity of ALHQG can beat the SQL. Figure 2 shows K as a function of $\beta\Omega$ at different gains G. In general, the enhancement factor K firstly decreases to a minimum value and then gradually increases with $\beta\Omega$. The sensitivity of ALHQG is always below the SQL at the optimal Sagnac phase marked by pink rhombus in each curve and denoted by $\Lambda(N_{in}, G)$. Meanwhile, the larger G is, the smaller K or the better rotation sensitivity $\Delta\Omega$ can be obtained. Furthermore, the optimal $\beta\Omega$ is closer to zero, which means that the rotation measurement is very sensitive to the change of the rotation rate. The enhancement of the sensitivity is accompanied with the decrease of the dynamic range of rotation measurement. In the future practical application, a balance between sensitivity and dynamic range should be considered.

Based on the above analysis, when $\beta\Omega$ is at the optimal point $\Lambda(N_{in}, G)$, we have $1 - \cos(\beta\Omega) \approx 0$ and

$\sin(\beta\Omega) \approx \Lambda(N_{in}, G)$. Due to $\beta = 2\pi DL/(\lambda c)$, the minimum rotation sensitivity $(\Delta\Omega)_{min}$ is

$$(\Delta\Omega)_{min} \approx \frac{\lambda c}{4\pi DL\sqrt{N_{in}} |Gg|^2 \Lambda(N_{in}, G)}, \tag{17}$$

where L is Sagnac loop length and λ is the wavelength. It can be seen that the larger N_{in}, G, and L are, the better $(\Delta\Omega)_{min}$. As shown in Fig. 3, $(\Delta\Omega)_{min}$ in the dark-yellow dashed line, can always beat the SQL illustrated by the red dash-dotted line.

However, in practice, the photon loss and atomic decoherence in the ALHQG can not be ignored. Based on Eq. (4), the photon number of the Stokes light is $\langle \hat{a}_2^\dagger \hat{a}_2 \rangle = e^{-\alpha_T L} \langle \hat{a}_1^\dagger \hat{a}_1 \rangle$. The photon number decreases with the loop length L at the rate of α_T. At the same time, based on Eq. (6), the atomic number of the spin wave is $\langle \hat{S}_2^\dagger \hat{S}_2 \rangle \simeq$
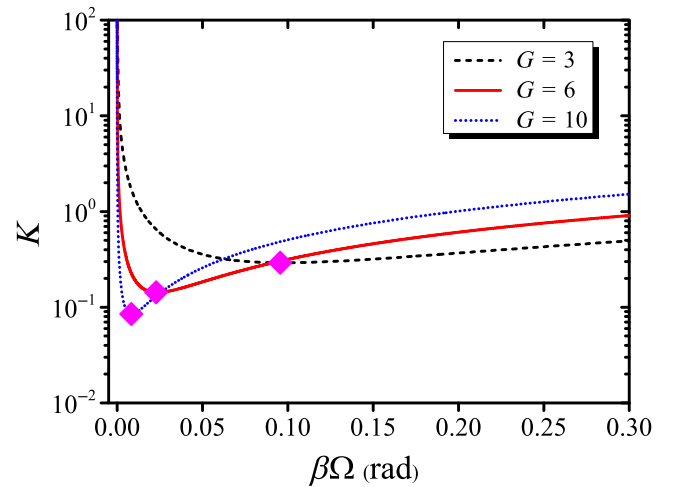

FIG. 2. Sensitivity enhancement factor K versus Sagnac phase $\beta\Omega$ with different gains G when $N_{in} = 10^8$ in a single shot.
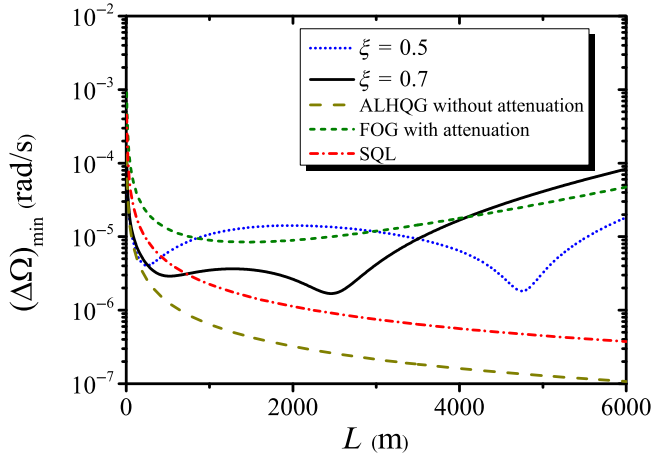
FIG. 3.   Minimum $\Delta\Omega$ versus loop length L with different attenuation coefficient ratios ξ when $G_1 = 6$, $N_{in} = 10^8$ in a single shot and $\alpha_T = 3$ dB/km.

$e^{-2\Gamma\tau}\langle\widehat{S}_1^\dagger\widehat{S}_1\rangle$. The atomic number also decreases with L at the rate of $2n\Gamma/c$ since $\tau = nL/c$ where n is the refractive index of the optical fiber. It is known that the attenuation leads to poor sensitivity due to the weaker quantum correlation [21]. Furthermore, due to the different attenuation rates of the light field (α_T) and atomic spin wave ($2n\Gamma/c$), the particle number of the interference arms in ALHQG are unequal. And thus, it is complex to analyze the dependence of the minimum rotation sensitivity $(\Delta\Omega)_{min}$ on the loop length and attenuation. To further study this dependence, we firstly define the attenuation coefficient ratio $\xi = 2n\Gamma/c/\alpha_T$, who is independent of loop length L. And then the influences of the loop length and attenuation are investigated in the following.

When the input particle number is $N_{in} = 10^8$ in a single shot and the gain is $G_1 = 6$ ($G_2 < G_1$ due to the photon loss of the Raman write beam), the relation between $(\Delta\Omega)_{min}$ and L with different ξ is shown in Fig. 3. As we can see, $(\Delta\Omega)_{min}$ has two optimal points. This is the result of the competition between the enhancement from the loop length and the reduction from the particle-number attenuation. When the loop length is small, the effect of attenuation is small. $(\Delta\Omega)_{min}$ is close to that in the ideal condition shown in the dark-yellow dashed line in Fig. 3. With the increase of the loop length, the attenuation in light and atom exponentially increases and leads to the first optimal point. And then, $(\Delta\Omega)_{min}$ decreases with L and reaches the second optimal point. Furthermore, we also give the sensitivity of the classical FOG (see Appendix) in the olive dashed line. It is calculated with the same rotation-sensitive particle number N_{tot} and the same optical loss as ALHQG. It can be seen that even with the attenuation, $(\Delta\Omega)_{min}$ of the ALHQG at the first optimal point can still beat the SQL $[1/(\beta\sqrt{N_{tot}})]$ and is better than the classical FOG. So we focus on the parameters of the first optimal point.

Moreover, the minimum rotation sensitivity $(\Delta\Omega)_{min}$ is also related with ξ. As shown in Fig. 3, $(\Delta\Omega)_{min}$ at $\xi = 0.5$ is worse than that at $\xi = 0.7$. When ξ is given, the minimum rotation sensitivity $(\Delta\Omega)_{min}$ at the optimal L can be obtained. The different ξ leads to different $(\Delta\Omega)_{min}$ at the different optimal L as shown in Fig. 4. Obviously, when $N_{in} = 10^8$ in a single shot, $G_1 = 6$, $\lambda = 795$ nm, $D = 0.2$ m, $\Lambda(G, N_{in}) = 0.02286$ rad, and $\alpha_T = 3$ dB/km, the attenuation coefficient rate should be optimized to $\xi = 0.7$ to get the minimum $\Delta\Omega = 2.905 \times 10^{-6}$ rad/s. In addition, a useful finding is that the optimal ξ increases with gain G_1, shown in Fig. 4. The reason is that there is only optical input field but no initial atomic spin wave at the input ports of the ALHQG. The best sensitivity should be achieved at the best interference visibility. Thus, the intensity balance of two interference arms is crucial. That is why the best visibility is always gotten when the decoherence of atomic beams is smaller than the loss of the optical field, and the attenuation coefficient rate ξ increases with gain G_1. Therefore, a tunable attenuation coefficient rate ξ is really essential in practice, but this is indicated by few works.

Finally, the ALHQG is built based on the optimal parameters obtained above. Based on this setup, the optimal rotation rate Ω_{opt} [$= \lambda c\Lambda(G_1, N_{in})/2\pi DL$] is determined. Using the above set of parameters, Fig. 5 shows a period of the dynamic range of ALHQG and the classical FOG (see Appendix). The ALHQG can beat SQL nearby the optimal rotation rate Ω_{opt}, while the classical FOG cannot. Furthermore, compared with the earth rotation rate $\Omega_e = 7.29 \times 10^{-5}$ rad/s, both ALHQG and FOG cannot work well in all rotation rates. The reason is that when the rotation rate deviates from the optimal rotation rate, the increasing of intensity noise leads to the degradation of the rotational sensitivity for both ALHQG and
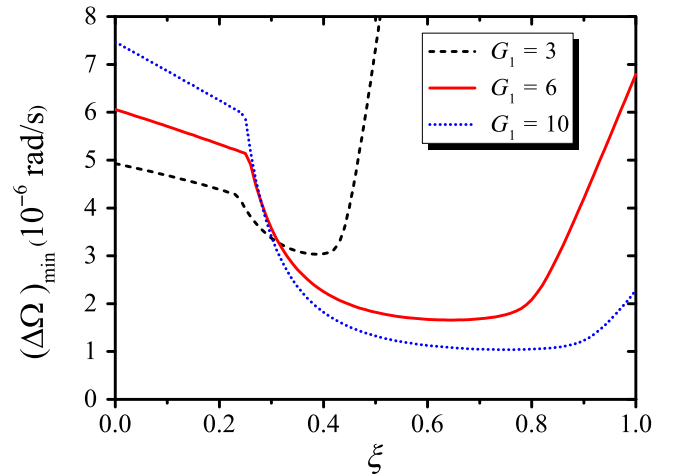

FIG. 4.   Minimum $\Delta\Omega$ versus the attenuation coefficient rate ξ with different gains G_1 when $N_{in} = 10^8$ in a single shot and $\alpha_T = 3$ dB/km.
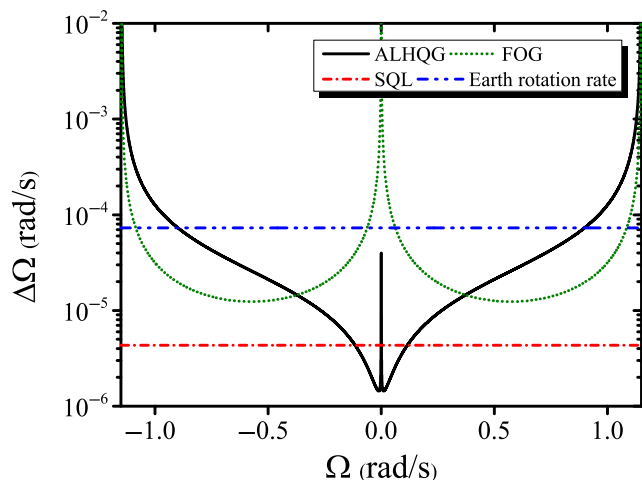
FIG. 5. Dynamic range. Parameters: $N_{in} = 10^8$ in a single shot, $G_1 = 6$, $\lambda = 795$ nm, $D = 0.2$ m, $\alpha_T = 3$ dB/km, $\xi = 0.7$, and $L = 520$ m. FOG has the same loop length and the same rotation-sensitive particle number.

FOG. Our proposed scheme can further increase the measured particle number to improve the rotation sensitivity, so that it can be better than the earth rotation rate in most dynamic ranges except for the divergence points and its vicinity.

Therefore, we analyze the dependence of the rotation sensitivity $\Delta\Omega$ on six parameters, N_{in}, G_1, L, Ω, α_T, and Γ. In general, $\Delta\Omega$ decreases with N_{in} and G_1 and increases with α_T and Γ. When N_{in}, G_1, α_T, and Γ are given, the minimum $\Delta\Omega$ can be obtained with the optimal fiber loop length L.

IV. DISCUSSION

The theoretical analysis based on real experimental parameters is useful to guide the future experimental realization. Now we present the experimental parameters to obtain the sensitivity of ALHQG [21]. The Raman-amplification process based on the ^{87}Rb ensemble is employed to realize the QBS(C). The wavelength of the lights is $\lambda = 795$ nm and the attenuation coefficient in optical fiber is $\alpha_T = 3$ dB/km. The input Stokes field is a 1-μs-long pulse with a repetition rate of 10 kHz and a power of 30 μW. When the gain is $G_1 = 6$, the diameter of the Sagnac loop is $D = 0.2$ m, the attenuation coefficient ratio is $\xi = 0.7$ and the length of the Sagnac loop is $L = 520$ m, the minimum sensitivity is 2.905×10^{-8} rad/s/$\sqrt{\text{Hz}}$.

In practical measurement, the sensitivity of the ALHQG may suffer from the instability of the laser, which mainly has an influence on N_{in}, $G_1 = \cosh(|\eta A_{p,1}| t)$, and $G_2 = \cosh(|\eta A_{p,2}| t)$ where $\eta \propto \Delta^{-1}$. The gain G_1 (or G_2) depend on the amplitude $A_{p,1}$ (or $A_{p,2}$) and the frequency detuning Δ of the strong Raman write beam. Based on Eq. (12), the fluctuations of N_{in}, G_1, and G_2 affect the rotation

sensitivity. Normally, the intensity fluctuation of the laser beam can be easily stabilized within $\pm 0.1\%$. And thus, the fluctuation of N_{in} causes the fluctuation of the rotation sensitivity between $2.904 \sim 2.907 \times 10^{-8}$ rad/s/$\sqrt{\text{Hz}}$. Furthermore, the frequency detuning Δ is about 1 GHz and its fluctuation is about 1 MHz. Thus, the intensity and the frequency fluctuation of the Raman write beam A_p are both within $\pm 0.1\%$, the corresponding gain G fluctuates between 5.9978 and 6.0272. The rotation sensitivity fluctuates between 2.903×10^{-8} rad/s/$\sqrt{\text{Hz}}$ and 2.907×10^{-8} rad/s/$\sqrt{\text{Hz}}$. It can be seen that the impact of the fluctuation of laser on the rotation sensitivity of ALHQG is smaller than 10^{-10} rad/s/$\sqrt{\text{Hz}}$.

V. CONCLUSION

We propose an ALHQG, where an atomic ensemble as QBS(C), and an optical Sagnac loop to couple the rotation rate. Under ideal condition, the value of the rotation sensitivity, decreasing monotonically with the Raman gain and Sagnac loop length, can beat the SQL because of the enhancement by Raman amplification. In the presence of the attenuation of the optical and atomic interference arms, the sensitivity has two optimal points as the Sagnac loop length increases. This is the result of the competition between the enhancement from the loop length and the reduction from the particle-number attenuation. At the first optimal point, the sensitivity can still beat the SQL. Furthermore, the minimum sensitivity of the ALHQG always surpasses that of the classical FOG with the same loop length and the same rotation-sensitive particle number.

The ALHQG can be operated without complicated phase locking. Compared with other kinds of gyroscopes, our gyroscope has advantages of simple structure, easy operation, and good sensitivity below the SQL. The theoretical analysis with practically experimental parameters shows that the sensitivity can reach 10^{-8} rad/s/$\sqrt{\text{Hz}}$, which is one order of magnitude better than that of the classical FOG. In future, the sensitivity can be improved further with larger input particle number, larger gain by increasing the optical depth of the atomic vapor cell. This ALHQG could find practical application in modern inertial navigation systems.

APPENDIX: THE SENSITIVITY ANALYSIS OF THE CLASSICAL FIBER OPTIC GYROSCOPE

In classical FOG [10], a coherent state enters into one port of the gyroscope, while a vacuum state enters into the other port. After passing through a 3-dB coupler, they propagate in the opposite directions inside a fiber Sagnac loop. As a result, the lights in CW and CCW experience a Sagnac phase induced by the rotation rate Ω. Hence, the final photon number is

$$\langle n \rangle_{\text{FOG}} = \frac{1}{2} T |\rho|^2 \left[1 + \cos(\beta \Omega) \right].$$

Here $|\rho|^2$ is the particle number of the input field in a single shot. $T = \exp(-\alpha_T L)$ is the transmission coefficient of the photons, where α_T is the attenuation coefficient. $\beta \Omega$ is the Sagnac phase, where $\beta = 2\pi D L/(\lambda c)$, D is the diameter of the Sagnac loop, L is the length of the Sagnac loop, and c is the speed of light in vacuum. Therefore, based on the error-propagation analysis [20], the rotation sensitivity of classical FOG in a single shot is

$$(\Delta \Omega)_{\text{FOG}} = \frac{1}{\frac{1}{2} T |\sin(\beta \Omega)| \beta \sqrt{|\rho|^2}} \propto \frac{1}{\beta \sqrt{|\rho|^2}}.$$

With the same rotation-sensitive photon number $N_{\text{tot}} = |\rho|^2$ and the same optical loss T as ALHQG, the rotation sensitivity can be calculated to compare with ALHQG and SQL.

[1] A. Lawrence, *Modern Inertial Technology* (Springer, New York, 1998).

[2] G. Sagnac, L'ether lumineux demontre par l'effect du vent relatif d'ether dans un interferometre en rotaion uniforme, C. R. Acad. Sci. **157**, 708 (1913).

[3] R. Anderson, H. R. Bilger, and G. E. Stedman, "Sagnac effect": A century of Earth-rotated interferometers, Am. J. Phys. **62**, 975 (1994).

[4] A. Kolkiran and G. S. Agarwal, Heisenberg limited Sagnac interferometry, Opt. Express **15**, 6798 (2007).

[5] B. Barrett, R. Geiger, I. Dutta, M. Meunier, B. Canuel, A. Gauguet, P. Bouyer, and A. Landragin, The Sagnac effects: 20 years of development in matter-wave interferometry, C. R. Physique **16**, 343 (2015).

[6] Jonathan P. Dowling, Correlated input-port, matter-wave interferometer: Quantum-noise limits to the atom-laser gyroscope, Phys. Rev. A **57**, 4736 (1998).

[7] T. L. Gustavson, P. Bouyer, and M. A. Kasevich, Precision Rotation Measurement with an Atom Interferometer Gyroscope, Phys. Rev. Lett. **78**, 2046 (1997).

[8] D. Savoie, M. Altorio, B. Fang, L. A. Sidorenkov, R. Geiger, and A. Landragin, Interleaved atom interferometry for high-sensitivity inertial measurements, Sci. Adv. **4**, 7948 (2018).

[9] I. Dutta, D. Savoie, B. Fang, B. Venon, C. L. Garrido Alzar, R. Geiger, and A. Landragin, Continuous Cold-Atom Inertial Sensor with 1 nrad/sec Rotation Stability, Phys. Rev. Lett. **116**, 183003 (2016).

[10] J. Nayak, Fiber-optic gyroscope: From design to production [Invited], Appl. Opt. **50**, E152 (2011).

[11] H. C. Lefevre, The Fiber-Optic Gyroscope (Artech House, Boston, London, 2014), 2nd ed.

[12] J. Lautier, L. Volodimer, T. Hardin, S. Merlet, M. Lours, F. Pereira Dos Santos, and A. Landragin, Hybridizing matter-wave and classical accelerometers, Appl. Phys. Lett. **105**, 144102 (2014).

[13] Pierrick Cheiney, Lauriane Fouche, Simon Templier, Fabien Napolitano, Baptiste Battelier, Philippe Bouyer, and Brynle Barrett, Navigation-Compatible Hybrid Quantum Accelerometer Using a Kalman Filter, Phys. Rev. Appl. **10**, 034030 (2018).

[14] F. Zimmer and M. Fleischhauer, Sagnac Interferometry Based on Ultraslow Polaritons in Cold Atomic Vapors, Phys. Rev. Lett. **92**, 253201 (2004).

[15] F. E. Zimmer and M. Fleischhauer, Quantum sensitivity limit of a Sagnac hybrid interferometer based on slow-light propagation in ultracold gases, Phys. Rev. A **74**, 063609 (2006).

[16] Moritz Mehment, Tobias Eberle, Sebastian Steinlechner, Henning Vahlbruch, and Roman Schnabel, Demonstration of a quantum-enhanced fiber Sagnac interferometer, Opt. Lett. **35**, 1665 (2010).

[17] Michael R. Grace, Christos N. Gagatsos, Quntao Zhuang, and Saikat Guha, Quantum-Enhanced Fiber-Optic Gyroscope Using Quadrature Squeezing and Continuous-Variable Entanglement, Phys. Rev. Appl. **14**, 034065 (2020).

[18] Matthias Fink, Fabian Steinlechner, Johannes Handsteiner, Jonathan P. Dowling, Thomas Scheidl, and Ruper Ursi, Entanglement-enhanced optical gyroscope, New J. Phys. **21**, 053010 (2019).

[19] J. Xin, J. Liu, and J. Jing, Nonlinear Sagnac interferometer based on the four-wave mixing process, Opt. Express **25**, 1350 (2017).

[20] A. M. Marino, N. V. Corzo Trejo, and P. D. Lett, Effect of losses on the performance of an SU(1,1) interferometer, Phy. Rev. A **86**, 023844 (2012).

[21] B. Chen, C. Qiu, S. Chen, J. Guo, L. Q. Chen, Z. Y. Ou, and W. Zhang, Atom-Light Hybrid Interferometer, Phys. Rev. Lett. **115**, 043602 (2015).

[22] Z. D. Chen, C. H. Yuan, H. Ma, D. Li, L. Q. Chen, Z. Y. Ou, and W. Zhang, Effects of losses in the atom-light hybrid SU(1,1) interferometer, Opt. Express **24**, 17766 (2016).